



Nanoscale

**Continuous Growth Phenomenon for Direct Synthesis of
Monodisperse Water-soluble Iron Oxide Nanoparticles with
Extraordinarily High Relaxivity**

Journal:	<i>Nanoscale</i>
Manuscript ID	NR-ART-02-2020-001552
Article Type:	Paper
Date Submitted by the Author:	24-Feb-2020
Complete List of Authors:	CHEAH, POHLEE; Jackson State University, Department of Chemistry, Physics and Atmospheric Science Cowan, Terriona; Jackson State University, Department of Chemistry, Physics and Atmospheric Science Zhang, Rong; Jackson State University, Department of Chemistry, Physics and Atmospheric Science Fatemi-Ardekani, Ali; University of Mississippi Medical Center, Department of Radiology Liu, Yongjian; Washington University in Saint Louis School of Medicine, Department of Radiology Zheng, Jie; Washington University in Saint Louis School of Medicine, Department of Radiology Han, Fengxiang; Jackson State University, Department of Chemistry, Physics and Atmospheric Science Li, Yu; Louisiana State University, Material Characterization Center Cao, Dongmei; Louisiana State University, Material Characterization Center Zhao, Yongfeng; Jackson State University, Department of Chemistry, Physics and Atmospheric Science

Continuous Growth Phenomenon for Direct Synthesis of Monodisperse Water-soluble Iron Oxide Nanoparticles with Extraordinarily High Relaxivity

*Pohlee Cheah,^a Terriona Cowan,^a Rong Zhang,^a Ali Fatemi-Ardekani,^b Yongjian Liu,^c Jie
Zheng,^c Fengxiang Han,^a Yu Li,^d Dongmei Cao,^d Yongfeng Zhao^{a*}*

^a Department of Chemistry, Physics and Atmospheric Science, Jackson State University,
Jackson, MS 39217, United States

^b Department of Radiology, University of Mississippi Medical Center, Jackson, MS 39217,
United States

^c Mallinckrodt Institute of Radiology, Washington University School of Medicine, St. Louis, MO
63110, United States

^d Material Characterization Center, Louisiana State University, Baton Rouge, LA 70803, United
States

KEYWORDS: Continuous growth, Iron oxide nanoparticles, Water soluble, Magnetic resonance
imaging

ABSTRACT

The direct synthesis of highly water-soluble nanoparticles has attracted intensive interest, but systematic size control has not been reported. Here, we developed a general method for synthesizing monodisperse water-soluble iron oxide nanoparticles with nanometer-scale size increments from 4 nm to 13 nm in a single reaction. Precise size control was achieved by continuous growth in an amphiphilic solvent, diethylene glycol (DEG), where growth step was separated from nucleation step by sequential addition of reactant. There was only one reactant in the synthesis, and no need for additional capping agents and reducing agents. This study reveals the “living growth” character of iron oxide nanoparticles synthesis in an amphiphilic solvent. The synthetic method shows high reproducibility. The as-prepared iron oxide nanoparticles are extremely water soluble without any surface modification. Surprisingly, the synthesized 9 nm iron oxide nanoparticles exhibit extremely high transversal and longitudinal relaxivities of $425 \text{ mM}^{-1} \cdot \text{s}^{-1}$ and $32 \text{ mM}^{-1} \cdot \text{s}^{-1}$ respectively, which is among the highest transversal relaxivity in the literature for sub-10 nm spherical nanoparticles. This study will not only shed light on the continuous growth phenomenon of iron oxide nanoparticles in amphiphilic solvent, but could also stimulate the synthesis and application of iron oxide nanoparticles. The continuous growth method could be further extended to other materials for the controlled synthesis of water-soluble nanoparticles.

Introduction

Iron oxide nanoparticles are very attractive due to their unique magnetic properties and excellent biocompatibility.^{1,2} They are useful in a wide range of applications, including magnetic separation, disease diagnosis, drug delivery, and magnetic hyperthermia treatment.³⁻⁵ The size of iron oxide nanoparticles plays a critical role in their magnetic properties and applications. In particular, one prominent application involves the development of high-performance contrast agents for noninvasive magnetic resonance (MR) imaging. A study has shown that increasing the size of iron oxide nanoparticles to 12 nm will lead to high transversal relaxivity (r_2) and improve sensitivity as contrast agents for T_2 weighted MR imaging.⁶ Recently, high longitudinal relaxivity (r_1) and low r_2 / r_1 ratio have been reported when the size of iron oxide nanoparticles is less than 4 nm, which can be used for T_1 weighted MR imaging.^{7,8} Because nanoparticles need to be water soluble for many of their applications, particularly for biomedical applications, developing new methods to synthesize water-soluble nanoparticles with nanometer-scale size control is significant both scientifically and technically.^{5,9,10}

Traditionally, the co-precipitation method has been utilized for synthesizing water-soluble iron oxide nanoparticles in aqueous solution. Due to the low reaction temperature, this method shows poor control in size, shape, and size distribution.¹¹⁻¹³ As an alternative production method, iron oxide nanoparticles have been synthesized in the polyols such as ethylene glycol (EG), diethylene glycol (DEG), triethylene glycol (TREG), and tetraethylene glycol (TEG).¹⁴⁻¹⁷ The polyols can dissolve both inorganic salts and organic compounds because of their high dielectric constant. In comparison to the co-precipitation method, nanoparticles produced using polyol-synthesis showed a narrower size distribution. The higher reaction temperature of polyols favors nanoparticles with a higher crystallinity and therefore higher magnetic properties. The surface of the prepared iron

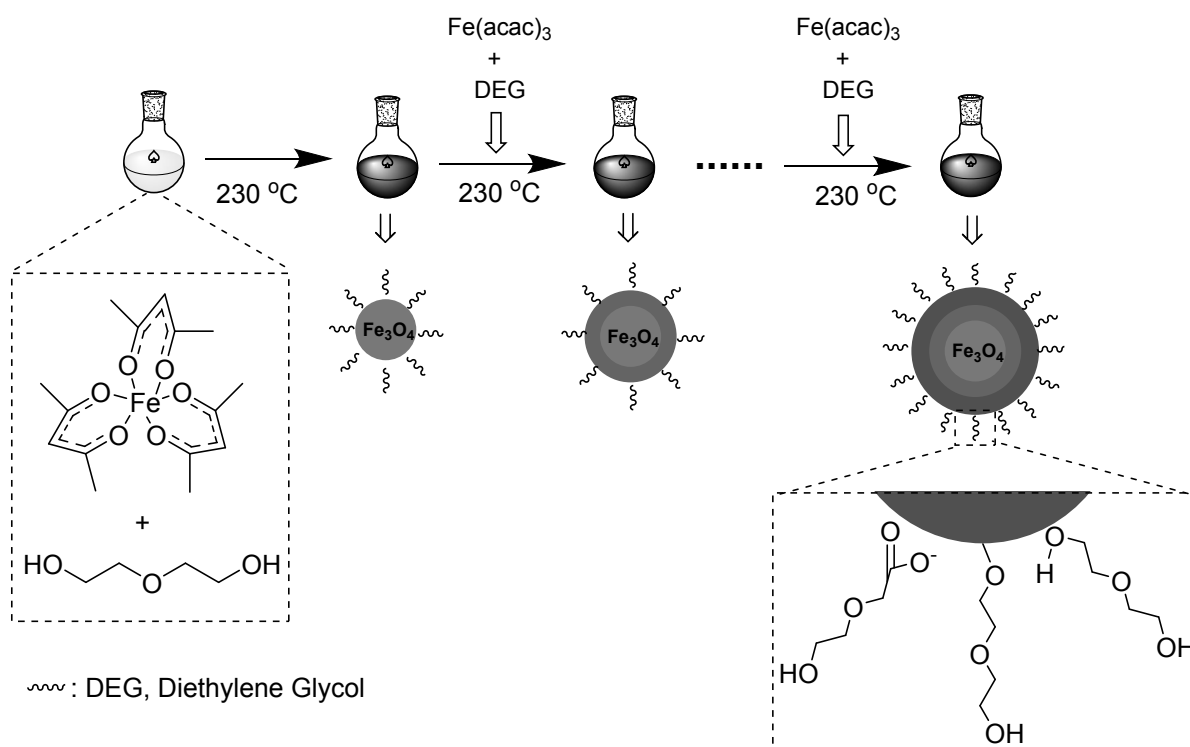
oxide nanoparticles is coated with hydrophilic polyol ligands in situ, allowing the nanoparticles to dissolve in aqueous solution.^{4,18} Because of its potential to synthesize water-soluble nanoparticles, there have been a variety of studies aiming to gain control on size.¹⁹⁻²¹ So far, systematic size control has not been achieved, in part because of fast nucleation and growth steps.¹⁷

The controlled synthesis of iron oxide nanoparticles has been significantly advanced by thermal decomposition method in nonpolar organic solvents.^{6,22} Due to the use of nonpolar organic solvents and relative high thermal stability of precursors, the growth step can be separated from the nucleation step. The size of nanoparticles can be manipulated by varying different organic solvents and aging time.²³ Furthermore, one nanometer-scale size control in the synthesis of monodisperse nanoparticles can be achieved by applying seed-mediated growth method with a typical size of about 6-12 nm.^{24,25} The systematic size control and reproducibility are further demonstrated by “living growth” methods.^{26,27} Nanoparticles can continue to grow when the precursor concentration is maintained in proper level. The “living growth” behavior makes it possible to manipulate size systematically, and synthesize sophisticated structures like core-shell structures using a straightforward procedure.²⁸ The synthesis of iron oxide nanoparticles with tunable sizes has greatly stimulated their applications.

However, a main challenge for the thermal decomposition method is that the as-prepared nanoparticles are only soluble in organic solvents.^{22,24} A sophisticated surface modification is required to render the water solubility. The overall strategy is to either attach an amphiphilic layer or replace hydrophobic layer with hydrophilic molecules.⁵ A variety of surface materials have been explored such as poly(acrylic acid),²⁹ poly(ethylene glycol)(PEG),³⁰ branched polymers,^{31,32} dopamine,^{33,34} zwitterions.³⁵ To obtain compact hydrodynamic size, small molecules are also explored for surface modification.^{23,35,36} However, due to the aggregation and low

reproducibility,³⁷ it has been an ongoing effort to improve the dispersity and stability of iron oxide nanoparticles in aqueous solution.

Scheme 1. General procedure for continuous growth of water-soluble iron oxide nanoparticles with nanometer-scale size increments.



To address the challenges of water solubility and systematic size control, this study reports the first continuous growth phenomenon of water-soluble iron oxide nanoparticles in an amphiphilic solvent (i.e. diethylene glycols). Similar to thermal decomposition method in nonpolar organic solvents, we hypothesize that the size of iron oxide nanoparticles can be precisely manipulated in diethylene glycol (DEG) once we can separate nucleation and growth step by simply sequential addition of reactant. The general strategy is outlined in **Scheme 1**. At controlled concentration, the reactant will decompose and add to the surface of the existing nanoparticles to form a larger one.

Growth from existing nanoparticles is thermodynamically preferred because the formation of new nuclei requires higher energy.^{38,39} Comparing to previous studies on synthesis of iron oxide nanoparticles in polyols,^{14,18} the novelty of this research is that a continuous growth phenomenon was discovered for the direct synthesis of water-soluble iron oxide nanoparticles in DEG. The as-prepared nanoparticles are highly water-soluble without any surface modification, and the size of monodisperse nanoparticles can be precisely tuned in nanometer-scale within broad size range.

Results and Discussion

To synthesize the iron oxide nanoparticles, commercially available $\text{Fe}(\text{acac})_3$ (acac = acetylacetonate) as the sole reactant was dissolved in DEG which recently has emerged as a versatile solvent for the synthesis of water-soluble nanoparticles.¹⁴⁻¹⁷ The $\text{Fe}(\text{acac})_3$ was selected as the reactant because it is soluble in DEG, and the decomposition temperature (186 °C) is lower than the boiling point of DEG (245 °C).⁴⁰ As a type of polyols, the DEG acts as both reducing agents and coating materials, so there is no need for extra capping agents such as oleic acid, oleic alcohol, and 1,2 hexadecanediol which are used in thermal decomposition method.²² Furthermore, the high boiling point of DEG (245 °C) can provide a high reaction temperature which is favored for high crystallinity of iron oxide nanoparticles.¹⁷

In the presence of argon, the reaction mixture was stirred at 120 °C for 1 h. Then, the reaction mixture was heated to 230 °C and allowed to react for 2 h. In order to increase the size of nanoparticles, the additional reactant was added to the reaction mixture slowly and the reaction mixture was stirred for another 2 h at the same temperature. The procedure of adding reactant was repeated for further growth of nanoparticles. To monitor the size, an aliquot of reaction mixture

was taken out before the reactant was added. The iron oxide nanoparticles readily dissolved in water without any surface modification after purification. The aqueous solutions of iron oxide nanoparticles were used for TEM measurement directly (**Figure 1**). As expected, TEM images clearly showed that the size of nanoparticles continuously grew as the reactant was added. Typically, the size of 4.0 ± 0.4 nm was obtained in the first 2 h (**Figure 1a**), and the size increased to 6.2 ± 0.5 nm after the reactant was added during the second time period (**Figure 1b**). After the sixth time period, the size of nanoparticles increased to 13 ± 1.3 nm (**Figure 1f**). The increase in size can be clearly observed by histograms from the size analysis of nanoparticles (**Figure 1S**). The large size we could obtain here is even bigger than that of nanoparticle prepared from conventional thermal decomposition method in nonpolar organic solvents.²⁷ The typical HRTEM images of the nanoparticles indicated that each nanoparticle is a well-defined single crystal, as shown in the insets of **Figure 1c** and **Figure 1f**. The defects are not observed in nanoparticles. The observation rules out the possibility that large size nanoparticles are formed from fusion of small size particles.

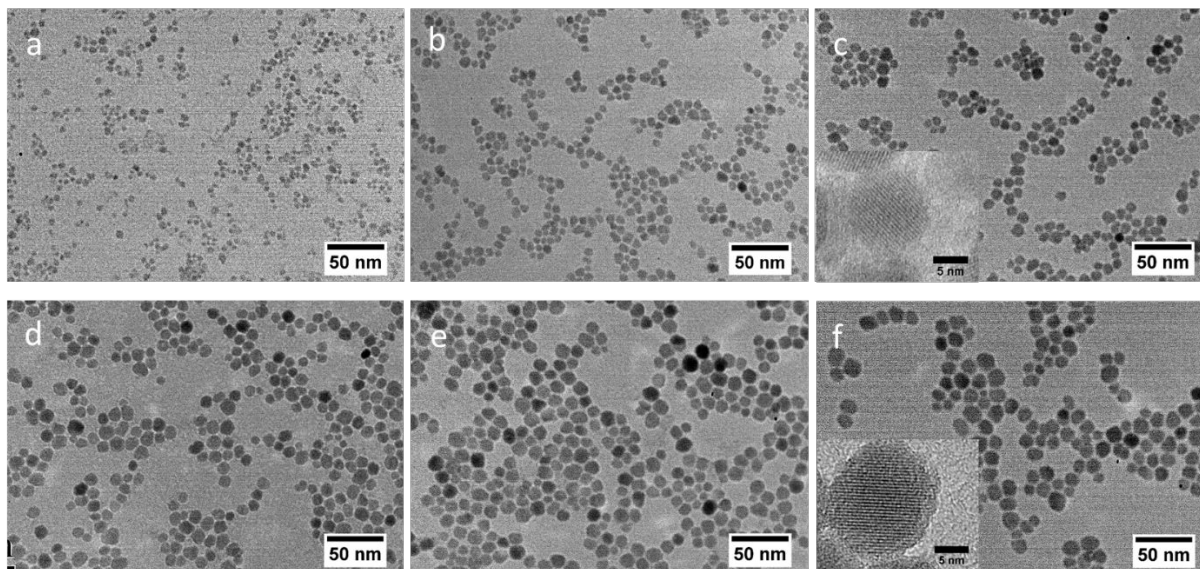


Figure 1. TEM images of iron oxide nanoparticles synthesized by continuous addition of starting materials. The average sizes are (a) 4.0 ± 0.4 nm, (b) 6.2 ± 0.5 nm, (c) 8.5 ± 0.9 nm, (d) 9.3 ± 1.1 nm, (e) 11.3 ± 1.1 nm, and (f) 13.0 ± 1.3 nm. Scale bars are 50 nm. Insets are high resolution TEM images in Figure 1c and 1f, showing single crystalline structures.

It is noteworthy that the size of obtained nanoparticles is uniform throughout the size range. The standard deviations in size are similar to that obtained in an organic solvent. For example, a typical size of this study was 8.5 ± 0.9 nm, while the similar size of 9.3 ± 0.7 nm was obtained in 1-octadecene.²⁷ The continuous growth synthesis is plausible largely due to the fact that the byproducts from $\text{Fe}(\text{acac})_3$ decomposition are gaseous and will escape from the reaction system.^{40,41} There is no accumulation of byproducts in the reaction system. In addition, $\text{Fe}(\text{acac})_3$ is the only reactant and no extra capping agents are needed in this reaction, which is different from the seed-mediated thermal decomposition method in organic solvent, where the capping agent and reducing agent need to be adjusted according to the progress of reaction.²⁷

Meade et al. reported that iron oxide nanoparticles with size of 3, 4, 5, and 6 nm can be synthesized by adjusting starting materials concentration and reaction time.¹⁸ In order to confirm that the size growth in this study was not caused by the possible time effect or Ostwald ripening process, a control reaction without addition of reactant was carried out to study time effect on size. A small amount of reaction mixture was removed for size measurement at 0.5 h, 1 h, 2 h, 3 h, 4 h, and 6 h. The TEM images are shown in **Figure S2**. From 0.5 h to 6 h, there was no obvious change in size. The result confirms that the size of iron oxide nanoparticles will not change if reactant is not added even though the reaction time is prolonged to 6 h. By monitoring the conversion rate of reactant in the reaction, we find that more than 90 % of $\text{Fe}(\text{acac})_3$ is converted into nanoparticles at 0.5 h. The average conversion rate is approximately 91 % from 1 h to 6 h. Both the high conversion rate and the unchanged size over time indicate that the Ostwald ripening is insignificant during the reaction.¹⁷ The results are consistent with our hypothesis that the size of nanoparticles grows by the addition of reactant.

This synthetic method is highly reproducible. **Figure S3** is typical TEM images for iron oxide nanoparticles synthesized from three individual reactions. For each reaction, additional reactant was added to synthesize iron oxide nanoparticles with three distinct sizes. From histograms made from size analysis by TEM in **Figure S4**, the increase of size was clearly observed when the reactant was added in sequence for each reaction. The sizes of nanoparticles from different reactions are summarized in **Table 1S**. For example, the sizes are 4.2 ± 0.7 nm, 6.9 ± 1.2 nm, and 9.5 ± 1.4 nm for nanoparticles in **Figure S3a-c** for the first reaction. There is no obvious size difference from reaction to reaction. Since the nucleation is a thermal dynamical process, it is possible that a slight size difference exists among different reactions. Our results show that the

sizes from different reactions are almost the same, implying that nucleation is not very sensitive to our reaction conditions.

The crystal structures of the nanoparticles were investigated by measuring their X-ray diffraction (XRD) patterns. **Figure 2** is the powder XRD patterns of iron oxide nanoparticles with three sizes (4 nm and 9 nm, and 13 nm). All of the diffraction peaks are indexed to the spinel structure known for magnetite.^{19,24,26,27} Because there is only a subtle difference between maghemite and magnetite phases, further studies will be performed to confirm the phase structure. With the increase in size, the peaks of XRD become sharper and intensity is stronger, indicating an increase in crystal domain. According to the Debye-Scherrer equation, the crystal domain sizes of iron oxide nanoparticles were calculated as 4.4 nm, 7.7 nm, and 10.3 nm respectively. The sizes are in good agreement with average diameters measured by TEM. Together with the HRTEM, the XRD study further confirmed that the nanoparticles have high crystallinity, and each nanoparticle is formed by a single crystal domain which is consistent with the mechanism of growth. That is the large nanoparticles are formed by continuous growing from the small nanoparticles after addition of reactant instead of an aggregation from small nanoparticles. For 13 nm nanoparticles, the calculated size from XRD is slightly smaller than that measured from TEM. This may be due to an amorphous layer outside of iron oxide nanoparticles shown in HRTEM. The amorphous layer may indicate that two-steps growth mechanism might involve in the synthesis.^{42,43} In the first step, the decomposition of iron (acac)₃ resulted in an iron based intermediate which attached to the surface of iron oxide nanoparticles to form an amorphous layer. In the second step, the amorphous layer further transformed into magnetite lattice. The detailed mechanism for this interesting synthesis is undergoing.

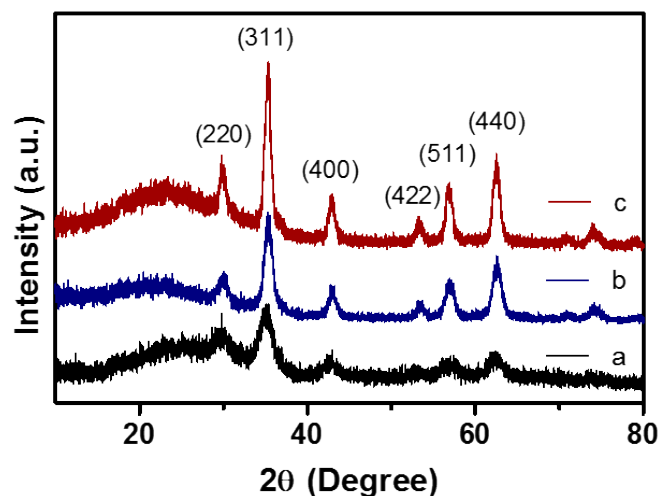


Figure 2. X-ray powder diffraction patterns of iron oxide nanoparticles with the size of (a) 4 nm; (b) 9 nm, (c) 13 nm.

One distinct advantage of this synthetic method is that iron oxide nanoparticles are water soluble immediately without sophisticated ligand exchange. All TEM images in this study were taken from aqueous solutions of as-prepared nanoparticles without a size-selection process. In these TEM images, the nanoparticles were well dispersed. The good water dispersity was further verified by plots of dynamic light scattering (DLS) (**Figure S5**). The single narrow peak reveals narrow size distribution. For iron oxide nanoparticles with core size of 9 nm, the hydrodynamic size increased slightly to 11.7 nm. The hydrodynamic size is relatively small when compared with nanoparticles synthesized by the thermal decomposition method followed by surface modification, which is in the range of 30 nm to 200 nm.^{34,37} The small hydrodynamic size indicates high water dispersity and compact coating materials on the surface of nanoparticles. In addition to core size, compact and thin surface coating materials are of great interest in order to reduce hydrodynamic size for

renal clearance,^{35,44-46} and increase the sensitivity of contrast agents by enhancing the interaction of the magnetic core with the surrounding water.⁴⁷

Furthermore, the nanoparticles have superior colloidal stability in aqueous solutions at different pHs. In **Figure 3a**, the iron oxide nanoparticles solutions are transparent without precipitation in acidic (5.4), neutral (7.4), and basic (9.0) phosphate buffer solution (PBS) after incubation for 7 days. During the procedure, the hydrodynamic sizes remained small and did not change obviously (**Figure 3b**). The high stability in aqueous solutions may be attributed to the surface charges which were confirmed by the zeta potential measurement.

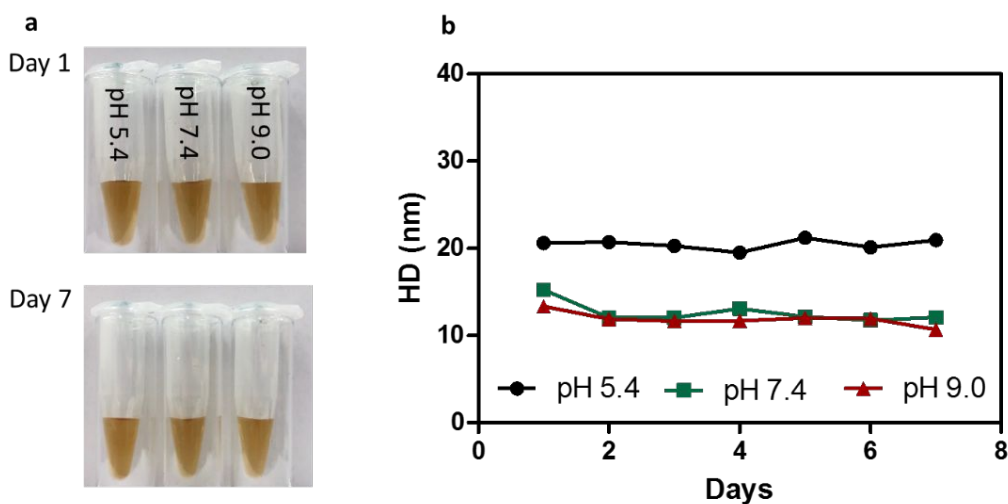


Figure 3. Colloid stability of iron oxide nanoparticles: (a) photographs, and (b) hydrodynamic size profiles of 9 nm iron oxide nanoparticles after incubation in PBS with pHs of 5.4, 7.4, and 9.0 for a week.

To explore the water solubility, the zeta-potential of as-prepared iron oxide nanoparticles were studied as the function of pH in water. As shown in **Figure 4**, the zeta potential is found to exhibit sigmoid curve which is consistent among different sizes. There is an isoelectric point at pH

between 5 and 6. Below the pH 5, the nanoparticles have positive charges (approx. 20 mV). Above pH 6, zeta potential is negative (approx. -30 mV). The sharp zeta potential transition is consistent with iron oxide nanoparticles synthesized in high molecular weight polyols.⁴⁸ The positive charge is probably from proton on the surface. The hydroxyl group on the end of DEG could form a chemical bond with surface $\text{Fe}^{2+}/\text{Fe}^{3+}$. The loosely bonded hydrogen atom could give positive charges on the surface.²⁰ The negative charge on the surface may be explained as a consequence of the progressive ionization of the hydroxyl end groups of DEG as pH increases.⁴⁹ Given the short chain, the stability of iron oxide nanoparticles may be due to the charges on the surface of nanoparticles.

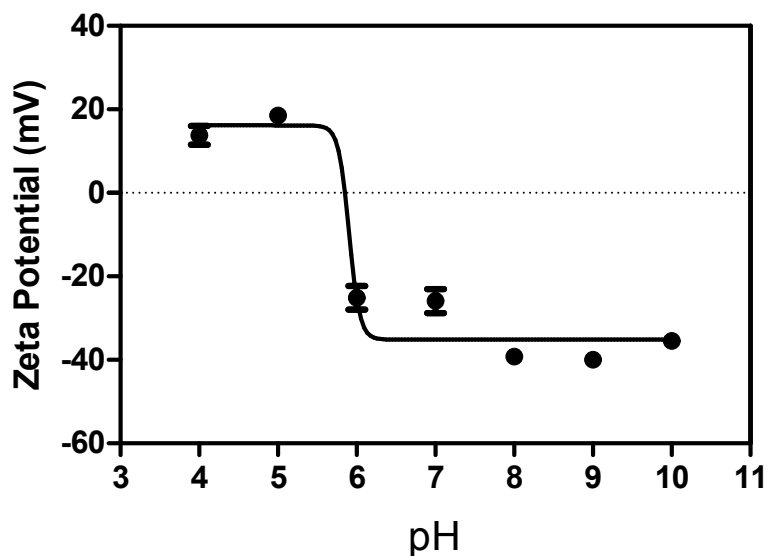


Figure 4. Zeta potential as function of pH for 9 nm iron oxide nanoparticles

Because there was excessive amount of DEG in the reaction system, we assume that the ligand on the surface of nanoparticles is DEG. To confirm this hypothesis, we examined the FT-IR spectrum of the organic layer on iron oxide nanoparticles. As illustrated in **Figure S6**, the characteristic peaks of 1070 cm^{-1} and 2927 cm^{-1} , attributed to C-O and C-H vibration of DEG, can

be seen in iron oxide nanoparticles.^{18,50} The broad absorption centered at 3338 cm^{-1} is from the stretching vibration of O-H from both DEG and absorbed water. As compared to DEG only, the vibration of Fe-O is observed in the absorption of 571 cm^{-1} ,²⁰ which indicates that these iron oxide nanoparticles could be magnetite (Fe_3O_4).^{14,18,19} In addition, the carboxylate groups are indicated because the FT-IR spectrum exhibits symmetric COO^- stretching at 1436 cm^{-1} , and asymmetric COO^- stretching at 1601 cm^{-1} .^{17,19,48}

To further explore the surface properties of iron oxide nanoparticles, the surface composition of iron oxide nanoparticles is studied by XPS. **Figure 5a** are wide scan XPS spectrum of 9 nm nanoparticles. The composition of Fe, C, and O can be identified. As shown in **Figure 5b**, the $\text{Fe}2p_{3/2}$ region of the spectrum can be fitted to three main peaks and two satellite peaks. The lowest binding energy peak at 710.1 eV is attributed to Fe^{2+} octahedral with a satellite peak at 714.6 eV . The Fe^{3+} octahedral peak is found at the peak with binding energy of 711.1 eV . The Fe^{3+} tetrahedral peak is assigned to the binding energy of 712.5 eV . The peak at binding energy of 718.6 eV is attributed to Fe^{3+} satellite.^{51,52} The presence of deconvolution peaks for both Fe^{2+} and Fe^{3+} confirms that the magnetite (Fe_3O_4) should be predominate phase.^{19,51-53}

As can be seen in **Figure 5c**, the high resolution O1s spectrum can be fit into 3 peaks of 530.3 , 531.1 , and 532.4 eV . The most intense peak at 530.3 eV is attributed to the lattice oxygen (Fe-O) in Fe_3O_4 .⁵¹ Monodentate oxygen moiety (i.e. C-O) gives rise to the peak at 531.1 eV , meanwhile bidentate carboxylate moiety ($\text{O}=\text{C}-\text{O}$) can be fitted to the peak at 532.4 eV .^{19,51} In C1s spectrum (**Figure 5d**), we observed the peak for alkyl carbon bond (C-C) (284.7 eV), C-O or C-OH (286.3 eV) and carboxylate moiety $\text{O}-\text{C}=\text{O}$ (288.2 eV) according to the literature.^{52,54}

Consistent with FT-IR, the XPS spectra from both C1s and O1s suggest the presence of carboxylate groups on the surface of iron oxide nanoparticles. The plausible reason is that polyols

is prone to be oxidized in raised temperature.^{48,55,56} The carboxylate group has been reported for the synthesis of iron oxide nanoparticles in polyols.¹⁹

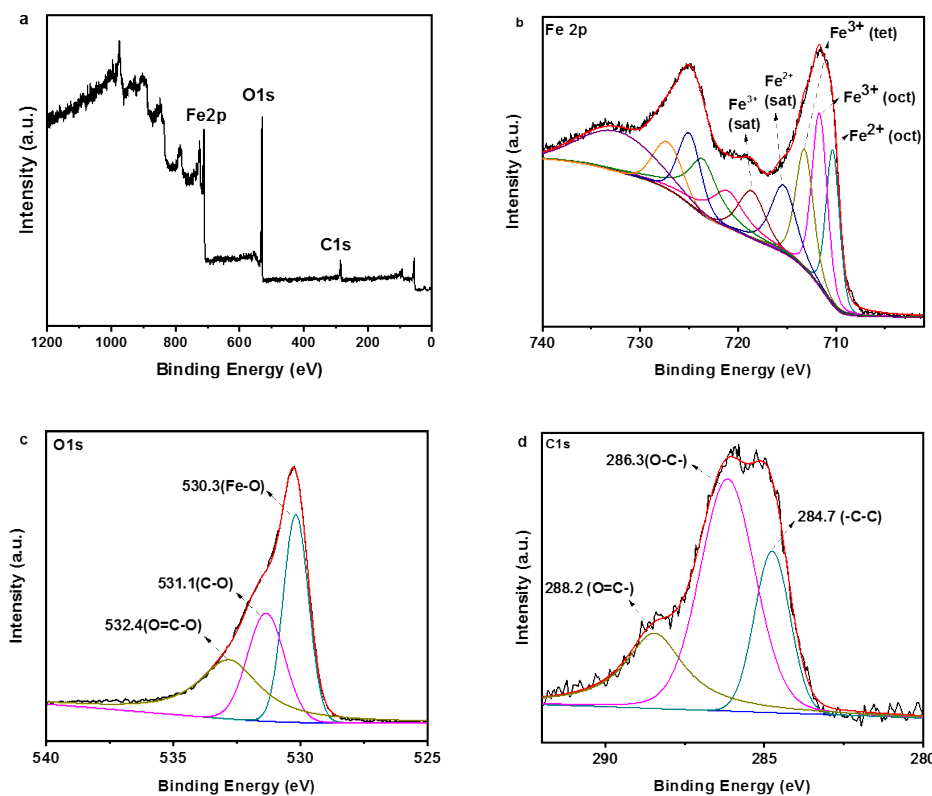


Figure 5. XPS spectra of 9 nm iron oxide nanoparticles: a) wide scan, b) Fe 2p, c) O1s, and d) C1s.

In order to study the density of DEG on the surface of iron oxide nanoparticles, we measured the weight of the organic layer on iron oxide nanoparticles by thermal gravimetric analysis (TGA). The TGA curves of iron oxide nanoparticles with three typical sizes are shown in **Figure S7**. The TGA curves showed a weight loss from 30 °C to 180 °C and then from 200 °C to 400 °C. The first stage at low temperature refers to the free DEG bonded to iron oxide nanoparticles and water absorbed on the surface.¹⁴ The second stage at higher temperature can be attributed to the

decomposition of DEG bonded to iron oxide nanoparticles via Fe-O bond. The weight loss curves are similar to iron oxide nanoparticles with a small size of 5 nm.⁵⁷ The weight losses after 180 °C are 12.7 %, 9.6 %, and 8.4 % for nanoparticles of 4 nm, 9 nm and 13 nm respectively. According to the density of iron oxide and molecular weight of DEG, we estimate that there are average 4.6 DEG molecules on every nm² surface for nanoparticles (**Table S2**). The density of the surface ligand is higher compared to the coverage of polyethylene glycols (PEG) on gold nanoparticles which is typically 1.6 molecules per nm².⁵⁸ When the size of the nanoparticles is smaller, the weight percentage of DEG in nanoparticles is higher. A similar trend was reported for hydrophobic iron oxide nanoparticles synthesized in an organic solvent.⁵⁹ A possible explanation is that the surface area to volume ratio increases when the size of nanoparticles decreases.^{59,60}

To study the magnetic behavior of iron oxide nanoparticles, the hysteresis loops of iron oxide nanoparticles was studied. **Figure 6** shows the hysteretic curve of 13 nm nanoparticles versus the applied field at 300 K and 5 K. At 300K, there is no remanence or coercivity and the nanoparticles are superparamagnetic. At 5K, the hysteresis loops show typical ferromagnetic behavior with a remanence of 26.4 emu.g⁻¹ and an estimated coercivity of 150 Oe. The saturated mass magnetization of the nanoparticles are found to be 77 emu.g⁻¹ and 68 emu.g⁻¹ at 5K and 300K, respectively. The high value of magnetization reported here is similar or even higher than the values measured for nanoparticles synthesized from non-continuous growth, proving that high quality magnetic nanoparticles can be synthesized by continuous growth.⁶¹ Because the weight of surface materials is included for calculating the magnetization, the saturated mass magnetization could be higher if the mass of surface materials is subtracted.

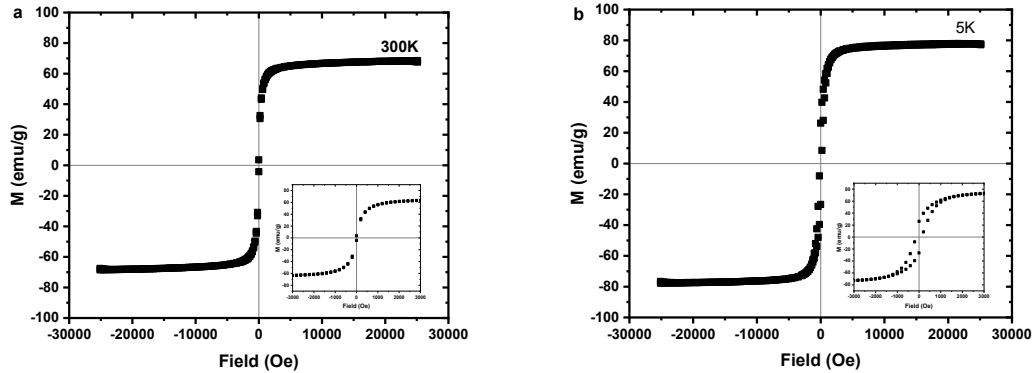


Figure 6. Magnetization as a function of magnetic field strength for 13 nm iron oxide nanoparticles at the temperature of a) 300 K and b) 5 K. Insert shows the data with an expanded scale from -3000 to 3000 Oe.

To study the effect of size on the magnetic behavior of iron oxide nanoparticles, the zero-field cooled (ZFC) and field cooled (FC) magnetization were measured in a magnetic field of 50 Oe in the temperature range from 5 K to 300 K. As shown in **Figure 7**, a maximum magnetization of $9.4 \text{ emu}\cdot\text{g}^{-1}$ is observed for the zero-field cooled (ZFC) curve of 13 nm iron oxide nanoparticles. The corresponding temperature is 258.9K, which is the blocking temperature (T_B). The blocking temperature are 80.3K, 123.3K, and 211.7K for nanoparticles with a size of 4 nm, 6 nm, and 9 nm, respectively. With an increase of size, the T_B increases.^{26,62,63} Consistent with M-H curve, the nanoparticles are superparamagnetic above T_B and ferromagnetic below T_B . Given the T_B value, the magnetic anisotropy constant K is calculated according to the equation: $K = 25 k_B T_B / V$, where k_B is the Boltzman constant ($1.38 \times 10^{-16} \text{ erg}\cdot\text{K}^{-1}$), T_B is measured blocking temperature, and V is the total volume of nanoparticles whose diameter was determined from TEM.²⁴ Assuming that the nanoparticles in this study are spherical in shape, the K for the size of 4 nm, 6 nm, 9 nm and 13 nm are calculated as 82.7, 37, 19, 7.7 ($\times 10^5 \text{ erg}\cdot\text{cm}^{-3}$) respectively. Compare to the magnetic

anisotropy constant²⁴ of 4×10^5 erg.cm⁻³ for bulk iron oxide, the K increases significantly with a reduction in size of nanoparticles. The trend is consistent with literature report.⁶² The increase of blocking temperature further confirmed continuous growth mechanism as the increase of T_B is consistent with the increasing domain size measured by TEM.^{24,26}

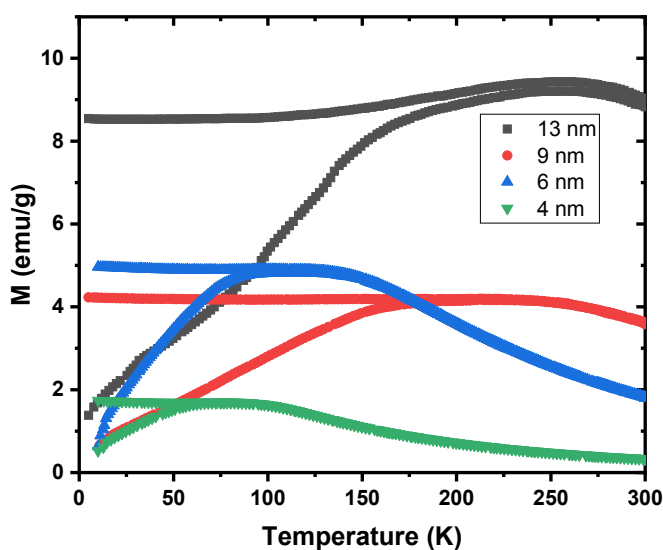


Figure 7. The magnetization as a function of temperature measured after zero-field cooled (ZFC) and field cooled (FC) under an applied field of 50 Oe for 4 nm, 6 nm, 9 nm, and 13 nm iron oxide nanoparticles.

Because of the superior colloidal stability and high crystallinity of synthesized iron oxide nanoparticles, we anticipate that they can be used for high-performance contrast agents for MR imaging. The MR imaging phantom study was conducted in order to evaluate the relaxivities. The iron oxide nanoparticles with high r_2 relaxivities will be detected at lower concentration and improve the sensitivity of MR imaging. **Figure 8a** shows the T_2 and T_1 weighted MR images of 9

nm iron oxide nanoparticles at different iron concentrations. With an increase in iron concentration, we can observe the dark signal enhancement in T_2 weighted MR imaging and bright signal enhancement in T_1 weighted MR imaging, implying that these iron oxide nanoparticles can act as both T_1 and T_2 contrast agents. By plotting the relaxation time as a function of iron concentration, the relaxivities (r_1 and r_2) were derived (**Figure 8b**). The relaxivities of different sizes are calculated and summarized in **Table S3**. Despite their relative small size, the r_1 and r_2 for 9 nm iron oxide nanoparticles are $32 \text{ mM}^{-1} \text{ s}^{-1}$ and $425 \text{ mM}^{-1} \text{ s}^{-1}$ respectively. It is noteworthy that the r_2 is higher than the highest r_2 of $385 \text{ mM}^{-1} \text{ s}^{-1}$ reported in literatures for the 13-15 nm spherical iron oxide nanoparticles.^{47,64} The r_2 value is comparable to that of the manganese doped iron oxide nanoparticles with a size of about 50 nm.⁶⁵ The contrast effect of iron oxide nanoparticles strongly depends on size. Both longitudinal and transversal relaxivities decrease with a decrease in size. When the size of iron oxide nanoparticles decreases to 4 nm, the r_1 and r_2 decrease to $23 \text{ mM}^{-1} \text{ s}^{-1}$ and $154 \text{ mM}^{-1} \text{ s}^{-1}$ respectively. With the decrease in size, we also notice that the transversal relaxivity decreases faster than that of longitudinal relaxivity, indicated by a decrease of r_2/r_1 ratio. This trend is consistent with other studies on size dependency.^{7,8,66}

The distinct r_2 relaxivity is probably due to high crystallinity, high water solubility, and a compact surface coating layer of iron oxide nanoparticles.^{65,67,68} According to the quantum-mechanical outer-sphere theory, the transversal relaxivity of iron oxide nanoparticles in solution can be calculated by the equation:^{47,69,70} $1/T_2 = (256\pi^2\gamma^2/405)V^* M_s^2 a^2/[D(1 + L/a)]$, where γ is the gyromagnetic ratio of proton; V^* , M_s , and a are the volume fraction, saturation magnetization, and the radius of iron oxide nanoparticles core, respectively; D is the diffusivity of water molecules, and L is the thickness of surface coating. If the total amount of iron (V^*) is

constant, the transversal relaxivity is predicted to increase with the increase of saturation magnetization and the effective diameter which will affect water surrounded outside nanoparticles. From magnetic property study, high saturation magnetization is observed for our iron oxide nanoparticles. The XRD demonstrated that iron oxide nanoparticles have high crystallinity which could result in the small dead region outside of iron oxide nanoparticles.⁶⁰ The high crystallinity is due to continuous growth procedure and high reaction temperature comparing to previous study in DEG.¹⁸ Meanwhile, the coating materials on the surface of our iron oxide nanoparticles are DEG molecules which are relatively short. As a result, the waters will have closer interactions with iron oxide nanoparticles and increase r_2 value.

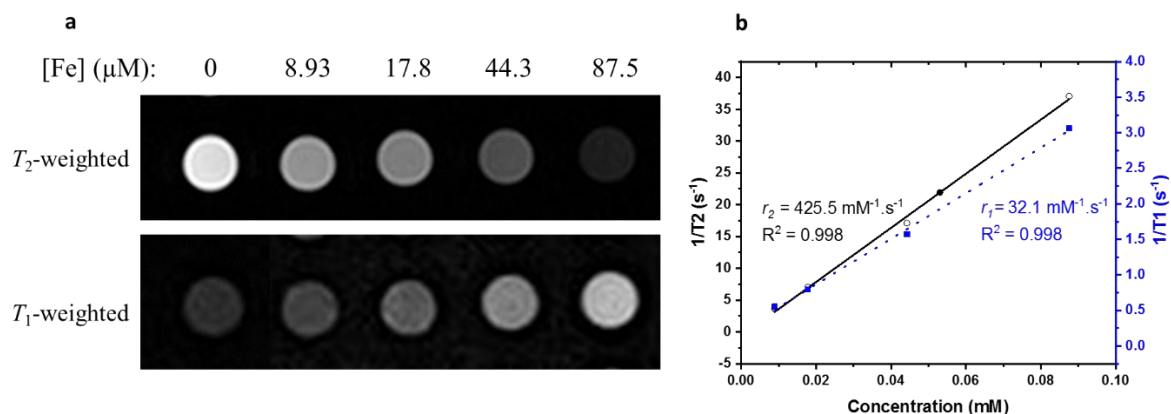


Figure 8. Magnetic resonance imaging phantom study and relaxivity under 1.5 T: (a) T_2 weighted and T_1 weighted MR phantom imaging of iron oxide nanoparticles; (b) The inverse of the T_2 weighted and T_1 weighted relaxation times as the function of iron concentrations.

Conclusions

In summary, this study has discovered a continuous growth behavior of water-soluble nanoparticles in amphiphilic solvent for the first time. The developed method not only grows iron

oxide nanoparticles with nanometer-scale size increment, but also provides high water solubility without any surface modification. The nanoparticles can keep growing step by step in nanometer-scale in DEG by simply adding reactant. The only reactant is $\text{Fe}(\text{acac})_3$ and there is no need for capping and reducing agents. The synthetic procedure is highly reproducible. The iron oxide nanoparticles synthesized here can disperse in water immediately without any surface modification. The aqueous solutions of iron oxide nanoparticles are stable at least one week. The nanoparticles are also found to have high crystallinity. More remarkably, the 9 nm iron oxide nanoparticles exhibit high transversal relaxivity (r_2) of $425 \text{ mM}^{-1} \cdot \text{s}^{-1}$ which is among the highest relaxivities for sub-10 nm spherical iron oxide nanoparticles in literature. They can potentially be used for high performance T_2 weighted contrast agents. The relaxivity properties are also strongly size-dependent. Although additional surface functionalization is necessary to conjugate targeting component and increase the biocompatibility, we reason the further surface functionalization can be easily completed in a homogeneous aqueous phase. For nanoparticles synthesized in organic phase, surface modification is hard partially because heterogeneous phase reactions are involved. Furthermore, the synthetic method can potentially be used to synthesize a series of water-soluble iron oxide nanoparticles with a continuous size spectrum under the same reaction conditions. These nanoparticles can serve as platform for the study of size-dependent physical properties. The concept of continuous growth in amphiphilic solvent could further be extended to other materials for the synthesis of highly water-soluble monodisperse nanoparticles with incremental sizes. Further studies are undergoing to fully understand the continuous growth mechanism in amphiphilic solvents and explore its applications.

Experimental Section

Chemicals and Materials

Iron (III) acetylacetonate ($\text{Fe}(\text{acac})_3$) $\geq 99.9\%$ and diethylene glycol (DEG) were purchased from Sigma-Aldrich (St. Louis, MO) and used without further purification.

Synthesis of iron oxide nanoparticles with controlled size. Typically, $\text{Fe}(\text{acac})_3$ (88 mg, 0.25 mmol) was mixed and stirred in 2.5 mL DEG (0.1 mmol Fe/ml) under argon gas exchange in a three-necked flask to obtain solution A. In another flask, $\text{Fe}(\text{acac})_3$ (530 mg, 1.5 mmol) was mixed in 15 mL DEG (0.1 mmol Fe/ml) and stirred under argon to obtain solution B. Both solutions were heated to 120 °C for an hour. Solution B was kept at 70 °C for future use. Solution A was further heated to 230 °C. After 2 hours, reaction mixture (0.5 ml) were taken out using glass syringe, and solution B (2.5 mL, 0.25 mmol) were added subsequently. The collection of reaction mixture and reactant addition were repeated for every 2 hours. After cooled down, the samples (50 μL) were mixed with 400 μL MilliQ water and purified by centrifugal filtration (Amicon, 30K) at 8000 rpm for 10 mins. MilliQ water was added to centrifugal filter and centrifuge again. This process was repeated for 3 times to get rid of excess DEG. The final products were dispersed in water and stored in room temperature for future use.

Synthesis of iron oxide nanoparticles without addition of reactant. In a typical reaction, $\text{Fe}(\text{acac})_3$ (247 mg, 0.7 mmol) was mixed with DEG (7 mL), and stirred under argon in a three-necked flask. Mixture was heated to 120 °C for an hour and further heated to 230 °C. The reaction mixture (0.5 mL) was collected using glass syringe at 0.5 h, 1 h, 2 h, 3 h, 4 h and 6 h of reaction time. After the samples cooled down, reaction mixture (50 μL) was mixed with 400 μL MilliQ water, and purified in centrifugal filtration (Amicon, 30K) at 8000 rpm for 10 mins. MilliQ water

was added to the mixture and centrifuge again. This process was repeated for 3 times to get rid of excess DEG.

ASSOCIATED CONTENT

Supporting Information

The following files are available free of charge.

Characterization and Measurements, TEM, Histograms, DLS, FT-IR, TGA, Table S1, Table S2, and Table S3 (PDF)

AUTHOR INFORMATION

Corresponding Author

*Email: yongfeng.zhao@jsums.edu

Notes

The authors declare no conflict of interest. Provisional patent application #62807407 filed with the United States Patent and Trademark Office

ACKNOWLEDGEMENTS

This research was supported by the National Science Foundation (grant number: HRD-1700390) and the NSF EPSCoR (grant number: OIA-1757220). We thank Qinku Zhang for an assistant with XRD experiments, and Ryan Dufrene for help with TGA measurement.

REFERENCES

- (1) Lee, N.; Yoo, D.; Ling, D.; Cho, M. H.; Hyeon, T.; Cheon, J. Iron Oxide Based Nanoparticles for Multimodal Imaging and Magnetoresponse Therapy. *Chemical Reviews* **2015**, *115*, 10637-10689.
- (2) Qiao, R.; Yang, C.; Gao, M. Superparamagnetic iron oxide nanoparticles: from preparations to in vivo MRI applications. *Journal of Materials Chemistry* **2009**, *19*, 6274-6293.
- (3) Tong, S.; Quinto, C. A.; Zhang, L.; Mohindra, P.; Bao, G. Size-Dependent Heating of Magnetic Iron Oxide Nanoparticles. *ACS Nano* **2017**, *11*, 6808-6816.
- (4) Wu, W.; Wu, Z.; Yu, T.; Jiang, C.; Kim, W.-S. Recent progress on magnetic iron oxide nanoparticles: synthesis, surface functional strategies and biomedical applications. *Science and Technology of Advanced Materials* **2015**, *16*, 023501.
- (5) Laurent, S.; Forge, D.; Port, M.; Roch, A.; Robic, C.; Vander Elst, L.; Muller, R. N. Magnetic Iron Oxide Nanoparticles: Synthesis, Stabilization, Vectorization, Physicochemical Characterizations, and Biological Applications. *Chemical Reviews* **2008**, *108*, 2064-2110.
- (6) Lee, J.-H.; Huh, Y.-M.; Jun, Y.-w.; Seo, J.-w.; Jang, J.-t.; Song, H.-T.; Kim, S.; Cho, E.-J.; Yoon, H.-G.; Suh, J.-S.; Cheon, J. Artificially engineered magnetic nanoparticles for ultra-sensitive molecular imaging. *Nature Medicine* **2006**, *13*, 95.
- (7) Kim, B. H.; Lee, N.; Kim, H.; An, K.; Park, Y. I.; Choi, Y.; Shin, K.; Lee, Y.; Kwon, S. G.; Na, H. B.; Park, J.-G.; Ahn, T.-Y.; Kim, Y.-W.; Moon, W. K.; Choi, S. H.; Hyeon, T. Large-Scale Synthesis of Uniform and Extremely Small-Sized Iron Oxide Nanoparticles for High-Resolution T1 Magnetic Resonance Imaging Contrast Agents. *Journal of the American Chemical Society* **2011**, *133*, 12624-12631.
- (8) Wei, H.; Bruns, O. T.; Kaul, M. G.; Hansen, E. C.; Barch, M.; Wiśniowska, A.; Chen, O.; Chen, Y.; Li, N.; Okada, S.; Cordero, J. M.; Heine, M.; Farrar, C. T.; Montana, D. M.; Adam, G.; Ittrich, H.; Jasanoff, A.; Nielsen, P.; Bawendi, M. G. Exceedingly small iron oxide nanoparticles as positive MRI contrast agents. *Proceedings of the National Academy of Sciences* **2017**.
- (9) Li, X.; Iocozzia, J.; Chen, Y.; Zhao, S.; Cui, X.; Wang, W.; Yu, H.; Lin, S.; Lin, Z. From Precision Synthesis of Block Copolymers to Properties and Applications of Nanoparticles. *Angewandte Chemie International Edition* **2018**, *57*, 2046-2070.
- (10) Bao, Y.; Sherwood, J. A.; Sun, Z. Magnetic iron oxide nanoparticles as T1 contrast agents for magnetic resonance imaging. *Journal of Materials Chemistry C* **2018**, *6*, 1280-1290.
- (11) Babes, L.; Denizot, B. t.; Tanguy, G.; Le Jeune, J. J.; Jallet, P. Synthesis of Iron Oxide Nanoparticles Used as MRI Contrast Agents: A Parametric Study. *Journal of Colloid and Interface Science* **1999**, *212*, 474-482.
- (12) Pileni, M. P. Nanocrystal Self-Assemblies: Fabrication and Collective Properties. *The Journal of Physical Chemistry B* **2001**, *105*, 3358-3371.
- (13) Jeong, J.-R.; Shin, S.-C.; Lee, S.-J.; Kim, J.-D. Magnetic properties of superparamagnetic γ -Fe₂O₃ nanoparticles prepared by coprecipitation technique. *Journal of Magnetism and Magnetic Materials* **2005**, *286*, 5-9.
- (14) Cai, W.; Wan, J. Facile synthesis of superparamagnetic magnetite nanoparticles in liquid polyols. *Journal of Colloid and Interface Science* **2007**, *305*, 366-370.
- (15) Feldmann, C.; Jungk, H.-O. Polyol-Mediated Preparation of Nanoscale Oxide Particles. *Angewandte Chemie International Edition* **2001**, *40*, 359-362.

- (16) Liu, J.; Sun, Z.; Deng, Y.; Zou, Y.; Li, C.; Guo, X.; Xiong, L.; Gao, Y.; Li, F.; Zhao, D. Highly Water-Dispersible Biocompatible Magnetite Particles with Low Cytotoxicity Stabilized by Citrate Groups. *Angewandte Chemie International Edition* **2009**, *48*, 5875-5879.
- (17) Ge, J.; Hu, Y.; Biasini, M.; Beyermann, W. P.; Yin, Y. Superparamagnetic Magnetite Colloidal Nanocrystal Clusters. *Angewandte Chemie International Edition* **2007**, *46*, 4342-4345.
- (18) Hu, F.; MacRenaris, K. W.; Waters, E. A.; Liang, T.; Schultz-Sikma, E. A.; Eckermann, A. L.; Meade, T. J. Ultrasmall, Water-Soluble Magnetite Nanoparticles with High Relaxivity for Magnetic Resonance Imaging. *The Journal of Physical Chemistry C* **2009**, *113*, 20855-20860.
- (19) Shen, L.-h.; Bao, J.-f.; Wang, D.; Wang, Y.-x.; Chen, Z.-w.; Ren, L.; Zhou, X.; Ke, X.-b.; Chen, M.; Yang, A.-q. One-step synthesis of monodisperse, water-soluble ultra-small Fe₃O₄ nanoparticles for potential bio-application. *Nanoscale* **2013**, *5*, 2133-2141.
- (20) Maity, D.; Kale, S. N.; Kaul-Ghanekar, R.; Xue, J.-M.; Ding, J. Studies of magnetite nanoparticles synthesized by thermal decomposition of iron (III) acetylacetonate in tri(ethylene glycol). *Journal of Magnetism and Magnetic Materials* **2009**, *321*, 3093-3098.
- (21) Hachani, R.; Lowdell, M.; Birchall, M.; Hervault, A.; Mertz, D.; Begin-Colin, S.; Thanh, N. T. K. Polyol synthesis, functionalisation, and biocompatibility studies of superparamagnetic iron oxide nanoparticles as potential MRI contrast agents. *Nanoscale* **2016**, *8*, 3278-3287.
- (22) Sun, S.; Zeng, H. Size-Controlled Synthesis of Magnetite Nanoparticles. *Journal of the American Chemical Society* **2002**, *124*, 8204-8205.
- (23) Park, J.; An, K.; Hwang, Y.; Park, J.-G.; Noh, H.-J.; Kim, J.-Y.; Park, J.-H.; Hwang, N.-M.; Hyeon, T. Ultra-large-scale syntheses of monodisperse nanocrystals. *Nature Materials* **2004**, *3*, 891.
- (24) Park, J.; Lee, E.; Hwang, N.-M.; Kang, M.; Kim, S. C.; Hwang, Y.; Park, J.-G.; Noh, H.-J.; Kim, J.-Y.; Park, J.-H.; Hyeon, T. One-Nanometer-Scale Size-Controlled Synthesis of Monodisperse Magnetic Iron Oxide Nanoparticles. *Angewandte Chemie International Edition* **2005**, *44*, 2872-2877.
- (25) Sun, S.; Zeng, H.; Robinson, D. B.; Raoux, S.; Rice, P. M.; Wang, S. X.; Li, G. Monodisperse MFe₂O₄ (M = Fe, Co, Mn) Nanoparticles. *Journal of the American Chemical Society* **2004**, *126*, 273-279.
- (26) Vreeland, E. C.; Watt, J.; Schober, G. B.; Hance, B. G.; Austin, M. J.; Price, A. D.; Fellows, B. D.; Monson, T. C.; Hudak, N. S.; Maldonado-Camargo, L.; Bohorquez, A. C.; Rinaldi, C.; Huber, D. L. Enhanced Nanoparticle Size Control by Extending LaMer's Mechanism. *Chemistry of Materials* **2015**, *27*, 6059-6066.
- (27) Cooper, S. R.; Plummer, L. K.; Cosby, A. G.; Lenox, P.; Jander, A.; Dhagat, P.; Hutchison, J. E. Insights into the Magnetic Properties of Sub-10 nm Iron Oxide Nanocrystals through the Use of a Continuous Growth Synthesis. *Chemistry of Materials* **2018**, *30*, 6053-6062.
- (28) Jansons, A. W.; Plummer, L. K.; Hutchison, J. E. Living Nanocrystals. *Chemistry of Materials* **2017**, *29*, 5415-5425.
- (29) Zhang, T.; Ge, J.; Hu, Y.; Yin, Y. A General Approach for Transferring Hydrophobic Nanocrystals into Water. *Nano Letters* **2007**, *7*, 3203-3207.

- (30) Kohler, N.; Fryxell, G. E.; Zhang, M. A Bifunctional Poly(ethylene glycol) Silane Immobilized on Metallic Oxide-Based Nanoparticles for Conjugation with Cell Targeting Agents. *Journal of the American Chemical Society* **2004**, *126*, 7206-7211.
- (31) Wang, W.; Ji, X.; Na, H. B.; Safi, M.; Smith, A.; Palui, G.; Perez, J. M.; Mattoussi, H. Design of a Multi-Dopamine-Modified Polymer Ligand Optimally Suited for Interfacing Magnetic Nanoparticles with Biological Systems. *Langmuir* **2014**, *30*, 6197-6208.
- (32) Liong, M.; Shao, H.; Haun, J. B.; Lee, H.; Weissleder, R. Carboxymethylated Polyvinyl Alcohol Stabilizes Doped Ferrofluids for Biological Applications. *Advanced Materials* **2010**, *22*, 5168-5172.
- (33) Xu, C.; Xu, K.; Gu, H.; Zheng, R.; Liu, H.; Zhang, X.; Guo, Z.; Xu, B. Dopamine as A Robust Anchor to Immobilize Functional Molecules on the Iron Oxide Shell of Magnetic Nanoparticles. *Journal of the American Chemical Society* **2004**, *126*, 9938-9939.
- (34) Amstad, E.; Gillich, T.; Bilecka, I.; Textor, M.; Reimhult, E. Ultrastable Iron Oxide Nanoparticle Colloidal Suspensions Using Dispersants with Catechol-Derived Anchor Groups. *Nano Letters* **2009**, *9*, 4042-4048.
- (35) Wei, H.; Insin, N.; Lee, J.; Han, H.-S.; Cordero, J. M.; Liu, W.; Bawendi, M. G. Compact Zwitterion-Coated Iron Oxide Nanoparticles for Biological Applications. *Nano Letters* **2012**, *12*, 22-25.
- (36) Jun, Y.-w.; Huh, Y.-M.; Choi, J.-s.; Lee, J.-H.; Song, H.-T.; KimKim; Yoon, S.; Kim, K.-S.; Shin, J.-S.; Suh, J.-S.; Cheon, J. Nanoscale Size Effect of Magnetic Nanocrystals and Their Utilization for Cancer Diagnosis via Magnetic Resonance Imaging. *Journal of the American Chemical Society* **2005**, *127*, 5732-5733.
- (37) Xu, Y.; Qin, Y.; Palchoudhury, S.; Bao, Y. Water-Soluble Iron Oxide Nanoparticles with High Stability and Selective Surface Functionality. *Langmuir* **2011**, *27*, 8990-8997.
- (38) Sun, Y.; Xia, Y. Shape-Controlled Synthesis of Gold and Silver Nanoparticles. *Science* **2002**, *298*, 2176-2179.
- (39) LaMer, V. K.; Dinegar, R. H. Theory, Production and Mechanism of Formation of Monodispersed Hydrosols. *Journal of the American Chemical Society* **1950**, *72*, 4847-4854.
- (40) Hoene, J. V.; Charles, R. G.; Hickam, W. M. Thermal Decomposition of Metal Acetylacetonates: Mass Spectrometer Studies. *The Journal of Physical Chemistry* **1958**, *62*, 1098-1101.
- (41) Jia, Q.; Zeng, J.; Qiao, R.; Jing, L.; Peng, L.; Gu, F.; Gao, M. Gelification: An Effective Measure for Achieving Differently Sized Biocompatible Fe₃O₄ Nanocrystals through a Single Preparation Recipe. *Journal of the American Chemical Society* **2011**, *133*, 19512-19523.
- (42) Iwamoto, T.; Kinoshita, T.; Takahashi, K. Growth mechanism and magnetic properties of magnetite nanoparticles during solution process. *Journal of Solid State Chemistry* **2016**, *237*, 19-26.
- (43) Grabs, I.-M.; Bradtmöller, C.; Menzel, D.; Garnweitner, G. Formation Mechanisms of Iron Oxide Nanoparticles in Different Nonaqueous Media. *Crystal Growth & Design* **2012**, *12*, 1469-1475.
- (44) Soo Choi, H.; Liu, W.; Misra, P.; Tanaka, E.; Zimmer, J. P.; Itty Ipe, B.; Bawendi, M. G.; Frangioni, J. V. Renal clearance of quantum dots. *Nature Biotechnology* **2007**, *25*, 1165.

- (45) Liu, W.; Choi, H. S.; Zimmer, J. P.; Tanaka, E.; Frangioni, J. V.; Bawendi, M. Compact Cysteine-Coated CdSe(ZnCdS) Quantum Dots for in Vivo Applications. *Journal of the American Chemical Society* **2007**, *129*, 14530-14531.
- (46) Wei, R.; Cai, Z.; Ren, B. W.; Li, A.; Lin, H.; Zhang, K.; Chen, H.; Shan, H.; Ai, H.; Gao, J. Biodegradable and Renal-Clearable Hollow Porous Iron Oxide Nanoboxes for in Vivo Imaging. *Chemistry of Materials* **2018**, *30*, 7950-7961.
- (47) Tong, S.; Hou, S.; Zheng, Z.; Zhou, J.; Bao, G. Coating Optimization of Superparamagnetic Iron Oxide Nanoparticles for High T2 Relaxivity. *Nano Letters* **2010**, *10*, 4607-4613.
- (48) Gonçalves, R. H.; Cardoso, C. A.; Leite, E. R. Synthesis of colloidal magnetite nanocrystals using high molecular weight solvent. *Journal of Materials Chemistry* **2010**, *20*, 1167-1172.
- (49) Miguel-Sancho, N.; Bomati-Miguel, O.; Colom, G.; Salvador, J. P.; Marco, M. P.; Santamaría, J. Development of Stable, Water-Dispersible, and Biofunctionalizable Superparamagnetic Iron Oxide Nanoparticles. *Chemistry of Materials* **2011**, *23*, 2795-2802.
- (50) Khoee, S.; Kavand, A. A new procedure for preparation of polyethylene glycol-grafted magnetic iron oxide nanoparticles. *Journal of Nanostructure in Chemistry* **2014**, *4*, 111.
- (51) Wilson, D.; Langell, M. A. XPS analysis of oleylamine/oleic acid capped Fe₃O₄ nanoparticles as a function of temperature. *Applied Surface Science* **2014**, *303*, 6-13.
- (52) Iacovita, C.; Stiuftuc, R.; Radu, T.; Florea, A.; Stiuftuc, G.; Dutu, A.; Mican, S.; Tetean, R.; Lucaciu, C. M. Polyethylene Glycol-Mediated Synthesis of Cubic Iron Oxide Nanoparticles with High Heating Power. *Nanoscale Research Letters* **2015**, *10*, 391.
- (53) Fujii, T.; de Groot, F. M. F.; Sawatzky, G. A.; Voogt, F. C.; Hibma, T.; Okada, K. In situ XPS analysis of various iron oxide films grown by NO₂ assisted molecular-beam epitaxy. *Physical Review B* **1999**, *59*, 3195-3202.
- (54) Mondini, S.; Cenedese, S.; Marinoni, G.; Molteni, G.; Santo, N.; Bianchi, C. L.; Ponti, A. One-step synthesis and functionalization of hydroxyl-decorated magnetite nanoparticles. *Journal of Colloid and Interface Science* **2008**, *322*, 173-179.
- (55) Yang, K. M.; Cho, H.-I.; Choi, H. J.; Piao, Y. Synthesis of water well-dispersed PEGylated iron oxide nanoparticles for MR/optical lymph node imaging. *Journal of Materials Chemistry B* **2014**, *2*, 3355-3364.
- (56) Uekawa, N.; Endo, M.; Kakegawa, K.; Sasaki, Y. Homogeneous precipitation of Cr³⁺-M²⁺ (M = Ni, Zn, Co, Cu) oxalate by oxidation of the polyethylene glycol-cation complex. *Physical Chemistry Chemical Physics* **2000**, *2*, 5485-5490.
- (57) Zhang, M.; Cao, Y.; Wang, L.; Ma, Y.; Tu, X.; Zhang, Z. Manganese Doped Iron Oxide Theranostic Nanoparticles for Combined T1 Magnetic Resonance Imaging and Photothermal Therapy. *ACS Applied Materials & Interfaces* **2015**, *7*, 4650-4658.
- (58) Xia, X.; Yang, M.; Wang, Y.; Zheng, Y.; Li, Q.; Chen, J.; Xia, Y. Quantifying the Coverage Density of Poly(ethylene glycol) Chains on the Surface of Gold Nanostructures. *ACS Nano* **2012**, *6*, 512-522.
- (59) Huang, J.-H.; Parab, H. J.; Liu, R.-S.; Lai, T.-C.; Hsiao, M.; Chen, C.-H.; Sheu, H.-S.; Chen, J.-M.; Tsai, D.-P.; Hwu, Y.-K. Investigation of the Growth Mechanism of Iron Oxide Nanoparticles via a Seed-Mediated Method and Its Cytotoxicity Studies. *The Journal of Physical Chemistry C* **2008**, *112*, 15684-15690.

- (60) Pereira, C.; Pereira, A. M.; Fernandes, C.; Rocha, M.; Mendes, R.; Fernández-García, M. P.; Guedes, A.; Tavares, P. B.; Grenèche, J.-M.; Araújo, J. P.; Freire, C. Superparamagnetic MFe₂O₄ (M = Fe, Co, Mn) Nanoparticles: Tuning the Particle Size and Magnetic Properties through a Novel One-Step Coprecipitation Route. *Chemistry of Materials* **2012**, *24*, 1496-1504.
- (61) Qu, H.; Caruntu, D.; Liu, H.; O'Connor, C. J. Water-Dispersible Iron Oxide Magnetic Nanoparticles with Versatile Surface Functionalities. *Langmuir* **2011**, *27*, 2271-2278.
- (62) Mohapatra, J.; Zeng, F.; Elkins, K.; Xing, M.; Ghimire, M.; Yoon, S.; Mishra, S. R.; Liu, J. P. Size-dependent magnetic and inductive heating properties of Fe₃O₄ nanoparticles: scaling laws across the superparamagnetic size. *Physical Chemistry Chemical Physics* **2018**, *20*, 12879-12887.
- (63) Papaefthymiou, G. C. Nanoparticle magnetism. *Nano Today* **2009**, *4*, 438-447.
- (64) Yang, L.; Wang, Z.; Ma, L.; Li, A.; Xin, J.; Wei, R.; Lin, H.; Wang, R.; Chen, Z.; Gao, J. The Roles of Morphology on the Relaxation Rates of Magnetic Nanoparticles. *ACS Nano* **2018**, *12*, 4605-4614.
- (65) Casula, M. F.; Conca, E.; Bakaimi, I.; Sathya, A.; Materia, M. E.; Casu, A.; Falqui, A.; Sogne, E.; Pellegrino, T.; Kanaras, A. G. Manganese doped-iron oxide nanoparticle clusters and their potential as agents for magnetic resonance imaging and hyperthermia. *Physical Chemistry Chemical Physics* **2016**, *18*, 16848-16855.
- (66) Huang, J.; Wang, L.; Zhong, X.; Li, Y.; Yang, L.; Mao, H. Facile non-hydrothermal synthesis of oligosaccharide coated sub-5 nm magnetic iron oxide nanoparticles with dual MRI contrast enhancement effects. *Journal of Materials Chemistry B* **2014**, *2*, 5344-5351.
- (67) Roca, A. G.; Veintemillas-Verdaguer, S.; Port, M.; Robic, C.; Serna, C. J.; Morales, M. P. Effect of Nanoparticle and Aggregate Size on the Relaxometric Properties of MR Contrast Agents Based on High Quality Magnetite Nanoparticles. *The Journal of Physical Chemistry B* **2009**, *113*, 7033-7039.
- (68) Ai, H.; Flask, C.; Weinberg, B.; Shuai, X.-T.; Pagel, M. D.; Farrell, D.; Duerk, J.; Gao, J. Magnetite-Loaded Polymeric Micelles as Ultrasensitive Magnetic-Resonance Probes. *Advanced Materials* **2005**, *17*, 1949-1952.
- (69) Brooks, R. A.; Moyny, F.; Gillis, P. On T₂-shortening by weakly magnetized particles: The chemical exchange model†. *Magnetic Resonance in Medicine* **2001**, *45*, 1014-1020.
- (70) Gillis, P.; Moyny, F.; Brooks, R. A. On T₂-shortening by strongly magnetized spheres: A partial refocusing model. *Magnetic Resonance in Medicine* **2002**, *47*, 257-263.

Table of Contents

A continuous growth phenomenon was discovered for synthesis of water-soluble iron oxide nanoparticles with nanometer-scale size control in an amphiphilic solvent. The as-prepared nanoparticles were extremely water soluble without any surface modification. Magnetic resonance imaging phantom studies show that the nanoparticles synthesized by this method had extraordinarily high transversal and longitudinal relaxivities compared to those of the same size prepared by the thermal decomposition method.

Continuous Growth of Water-soluble Nanoparticles

